Journal of Hazardous Materials 209–210 (2012) 478–483

Contents lists available at SciVerse ScienceDirect

Journal of Hazardous Materials

journal homepage: www.elsevier.com/locate/jhazmat

Preparation and characterization of hydrophobic Pt–Fe catalysts with enhanced catalytic activities for interface hydrogen isotope separation

Sheng Hu*, Jingwei Hou, Liangping Xiong, Kuiping Weng, Xingbi Ren, Yangming Luo

Institute of Nuclear Physics and Chemistry, China Academy of Engineering Physics, Mianyang 621900, China

ARTICLE INFO

Article history:
Received 2 October 2011
Received in revised form 17 January 2012
Accepted 17 January 2012
Available online 24 January 2012

Keywords:
Hydrophobic catalyst
Liquid phase catalytic exchange
Hydrogen isotope separation
Pt–Fe/C
Pt–Fe alloy

ABSTRACT

Liquid phase catalytic exchange reactions are mainly used for separation of hydrogen isotopes from liquid water. Based on the carbon-supported Pt and Pt–Fe catalysts, different hydrophobic Pt and Pt–Fe catalysts were fabricated for use in such reactions. The characterization results indicated the Pt–Fe alloy was formed in the Pt_3Fe/C catalyst prepared using a citric-acid-assisted $NaBH_4$ reduction method (CA-$NaBH_4$). However, there were more Fe oxide species and the Fe components existed independently in the Pt_3Fe/C catalyst prepared by the modified microwave-irradiated ethyl glycol reduction procedure (MI). Performance tests demonstrated that the activities of the hydrophobic Pt–Fe catalysts with appropriate Fe/Pt ratios, using the MI method, were enhanced because of the addition of Fe. In contrast, the hydrophobic Pt_3Fe catalyst prepared using the CA-$NaBH_4$ method had lower catalytic activity than pure Pt. Possible reasons were explained by reaction mechanisms of double routes of LPCE catalysis.

© 2012 Elsevier B.V. All rights reserved.

1. Introduction

Large amounts of tritiated water are unavoidably produced during activities such as spent-fuel reprocessing, the operation of heavy-water reactors, and the operation of fusion reactors in the future [1–11]. From the viewpoints of safety and economy, tritium recovery from this tritiated water is necessary. Liquid phase catalytic exchange (LPCE), i.e. hydrogen isotope exchange between liquid water and gaseous hydrogen, is an efficient reaction for separation of tritium from tritiated water [1–4]. This procedure has lower energy consumption and higher equilibrium separation factors for hydrogen isotopes than those of conventional vapor phase catalytic exchange reactions [1–4]. Hydrophobic catalysts are used in LPCE. Because of the waterproofing property of the hydrophobic catalyst, the reactions can proceed smoothly [5–11].

Pt, which is expensive, is widely accepted as the most active metal for LPCE and now is mainly used for preparation of the hydrophobic catalysts. Some efforts have been made to reduce the use of Pt in hydrophobic catalysts. A major approach is to optimize the method of fabricating the hydrophobic catalysts and to prepare highly dispersed Pt-based catalysts [5,7]. Another approach to reducing preparation costs is the addition of an appropriate amount of other components, such as Ir, Ru, Cr, or Ti [5,6,10]. The LPCE catalytic activities of Pt–Ir-alloy catalysts, with appropriate Pt/Ir molar ratios, are higher than those of catalysts containing only Pt [5]. However, the introduction of Ru, either as an alloy or as a hydrous oxide, can improve the catalytic activity of pure Pt [6]. Li also reported that the LPCE catalytic activities of Pt–Cr and Pt–Ti catalysts are higher than those of Pt catalysts [10]. Moreover, Pt–Ti catalysts exhibit good stability.

Recently, carbon-supported Pt–Fe catalysts have been intensively studied for use in fuel cells [12–15]. Pt–Fe alloy catalysts were found to have good electrocatalytic performances for methanol, ethanol, and formic acid electrooxidation [12–14]. The activities of Pt/C catalysts toward oxygen reduction reactions can also be increased by controlling the Pt particle size, using $FeCl_3$ as an additive [15]. The Fe existed only as impurities, not in an alloyed form in the Pt–Fe/C catalysts.

In our study, Fe was introduced into pure Pt to fabricate hydrophobic catalysts. First, carbon-supported Pt and alloying and non-alloying Pt–Fe catalysts were prepared by two different methods. The carbon-supported catalysts were then loaded onto an inert carrier to obtain hydrophobic catalysts. Polytetrafluoroethylene (PTFE) with a low surface energy was used to waterproof the catalyst. Finally, the LPCE activities of the hydrophobic Pt and Pt–Fe catalysts were tested and compared. The effects of Pt–Fe alloying and compositions on LPCE catalytic activities were investigated in detail. The reasons for the increased activities were analyzed.

2. Experimental

2.1. Synthesis of Pt/C and Pt–Fe/C catalysts

Carbon-supported Pt and Pt–Fe were prepared by two synthesis strategies, namely microwave-irradiated ethyl glycol (EG) reduction (MI) and citric-acid-assisted $NaBH_4$ reduction (CA-$NaBH_4$).

* Corresponding author. Tel.: +86 816 2494379; fax: +86 816 2495280.
E-mail address: husheng@126.com (S. Hu).

0304-3894/$ – see front matter © 2012 Elsevier B.V. All rights reserved.
doi:10.1016/j.jhazmat.2012.01.058

$H_2PtCl_6{\cdot}6H_2O$ and $FeCl_2{\cdot}4H_2O$ were used as precursors of the Pt and Pt–Fe catalysts, and Vulcan XC-72R carbon black (Cabot Corp., Boston, MA, USA) was used as the catalyst support. The Pt contents of all the carbon-supported Pt and Pt–Fe catalysts were fixed at 20 wt%. The obtained catalysts were denoted by Pt-preparation method or Pt–Fe-preparation method. Thus, Pt-MI corresponds to the Pt/C catalyst prepared by the MI method.

For the MI synthesis [5,6], 300 mg of carbon were ultrasonically dispersed in 30 mL of EG, followed by addition of an EG solution of the precursors to the suspension under constant stirring. The pH of the mixture was adjusted to 12.3 using a 1 mol L^{-1} NaOH aqueous solution. The synthesis solution was heated to 190 °C at a heating rate of 140 K min^{-1} in a closed ETHOS T microwave labstation (Milestone Inc.). The temperature was then maintained at 190 °C for 5 min. After cooling to ambient temperature, the resulting carbon-supported catalyst was filtered and washed with copious amounts of water. The collected catalyst was dried at 105 °C for 4 h.

For the CA-$NaBH_4$ procedure, 600 mg of carbon, and the precursor and sodium citrate in a molar ratio of 1/10 were ultrasonically dispersed in 100 mL of EG. The pH of the synthesis solution was adjusted to 8. After constant stirring for 1 h, the mixture was heated to 60 °C. A fresh $NaBH_4$ aqueous solution was added to the solution under stirring. Stirring was continued for another 2 h. After cooling to ambient temperature, the resulting catalyst powder was filtered, washed, and dried.

2.2. Characterization of carbon-supported catalysts

X-ray diffraction (XRD) analyses were carried out using a DX-2600 SSC diffractometer (Cu Kα radiation, λ = 1.5405 Å) at a scanning rate of 1.2° min^{-1} from 10° to 90°. Transmission electron microscopy (TEM) images were obtained with a JEOL JEM 3010 transmission electron microscope operated at 300 kV. X-ray photoelectron spectroscopy (XPS) analyses were performed on an ESCALAB 250 spectrometer. Narrow-scan photoelectron spectra of Pt 4f and Fe 3p were recorded and deconvoluted by XPSPEAK (version 4.1).

2.3. Fabrication of hydrophobic catalysts

As described in our previous work [5–7], a porous foamed-nickel (FN) material (2.5 mm thick, 110 PPI, 500 g m^{-2}) was used as an inert carrier for the hydrophobic catalysts. First, a stable slurry of the carbon-supported catalyst and polytetrafluoroethylene (PTFE) was prepared. The mixed slurry was then loaded onto the FN carrier, followed by drying and calcining at different temperatures to produce the hydrophobic catalyst. PTFE is used to bind the carbon-supported catalyst with the FN and to waterproof the catalyst. The hydrophobic catalysts were denoted by Pt-preparation method-H or Pt–Fe-preparation method-H.

2.4. Hydrophobic catalyst activity tests

Hydrophobic catalyst activity measurements were performed in a jacketed glass column of internal diameter 16 mm. Thermostatically controlled water (50 °C) was passed through the glass jacket to maintain a constant temperature over the column. The hydrophobic catalyst and an inert packing of Dixon phosphor bronze gauze rings were mixed homogeneously and used to fill the column. The volume ratio of the catalyst to the packing was 1/4. Deuterated water (D/H atomic ratio = 2.30×10^{-2}) and natural hydrogen steam (D/H atomic ratio = 1.36×10^{-4}) were fed into the reaction column counter-currently. The HD concentrations in the hydrogen gas at the reaction column inlet and outlet were analyzed with an Agilent 6890N gas chromatograph. The catalytic performance was evaluated by the column efficiency η of the isotope-exchange column [5–7].

3. Results and discussion

3.1. Characterization of carbon-supported catalysts

Pt/C and Pt–Fe/C catalysts were prepared, using the MI and CA-$NaBH_4$ methods. After the synthesis reaction and filtration, the filtrate was all colorless and transparent for the two processes. This indicates that the $PtCl_6^{2-}$ and Fe^{2+} ions reacted almost completely, and that the obtained particles were mostly loaded onto the carbon carrier.

TEM images of the resulting catalysts and the corresponding particle size histograms, based on analysis of more than 200 nanoparticles, are shown in Fig. 1. Most of the Pt and Pt–Fe nanoparticles were uniformly dispersed on the surface of the carbon supports in all these catalysts. For the MI procedure, the mean particle sizes were all small (1.9 nm for the pure Pt catalyst; 2.0 nm for the Pt_4Fe catalyst; 2.0 nm for the Pt_3Fe catalyst; 2.1 nm for the Pt_2Fe catalyst; and 2.4 nm for the PtFe catalyst), and highly dispersed Pt and Pt–Fe catalysts were obtained. The Pt–Fe particle size increased with increasing Fe/Pt atomic ratio. The majority of the Pt particles varied from 0.5 to 3.5 nm for Pt-MI. However, some metal particles ranging from 4 nm to 5.5 nm in size can be observed for PtFe-MI. This indicates that the particle size distribution broadened with the addition of Fe.

The MI method has been widely used for preparing different carbon-supported Pt-based catalysts [5,6,16–19]. It has been reported that the heating rate and the pH of the synthesis solution are two important influencing factors on the dispersion of the resulting catalyst [5]. A very fast heating rate and increased pH commonly produce highly dispersed catalysts. In this procedure, EG acts as the reducing agent. The Pt and Fe precursors are reduced to metallic Pt and Fe at high temperatures and the solution quickly becomes supersaturated with Pt and Fe metals. Metallic nuclei are thus formed and further grain growth results in the formation of nanoparticles. A very fast heating rate results in high supersaturation and a large number of nuclei; consequently, the particle sizes are small. EG is mainly oxidized to glycolic acid. However, glycolate, not glycolic acid, is a good stabilizer for metallic nanoparticles [18,19]. The glycolate concentration decreases with decreasing synthesis solution pH. Therefore, the particle sizes of the resulting catalysts decrease with increasing reaction solution pH. In this work, the Pt and Pt–Fe catalysts were prepared at a pH of 12.3 and at a very fast heating rate of 140 K min^{-1}. Thus, highly dispersed Pt and Pt–Fe particle sizes were obtained.

$NaBH_4$ reduction is also a conventional preparation method for carbon-supported catalysts [20–24]. Generally, the metallic catalysts obtained have large particle sizes. For the CA-$NaBH_4$ method, EG was used as the reaction solvent, instead of methanol, ethanol, or water [20]. EG is also an excellent dispersing medium for metal particles. The $[PtCl_6]^{2-}$ and Fe^{2+} ions were reduced to metallic Pt and Fe by the $NaBH_4$. CA, a stabilizer of the Pt and Pt–Fe particles, was introduced to decrease the Pt and Pt–Fe nanoparticle sizes [20,23]. During the reduction process, three carboxyl anions of CA were adsorbed on these metal nanoparticles. As a result, the repulsive forces between the negatively charged particles prevented particle growth and agglomeration [23]. Pt-MI and Pt_3Fe-MI were therefore more highly dispersed than the catalysts prepared by the ordinary $NaBH_4$ reduction method. However, EG cannot be reduced to glycolic acid at the reaction temperature (60 °C) used in the CA-$NaBH_4$ method, and hence CA was the only stabilizer. Fig. 1 shows that the mean nanoparticle sizes of the two catalysts were 2.3 nm

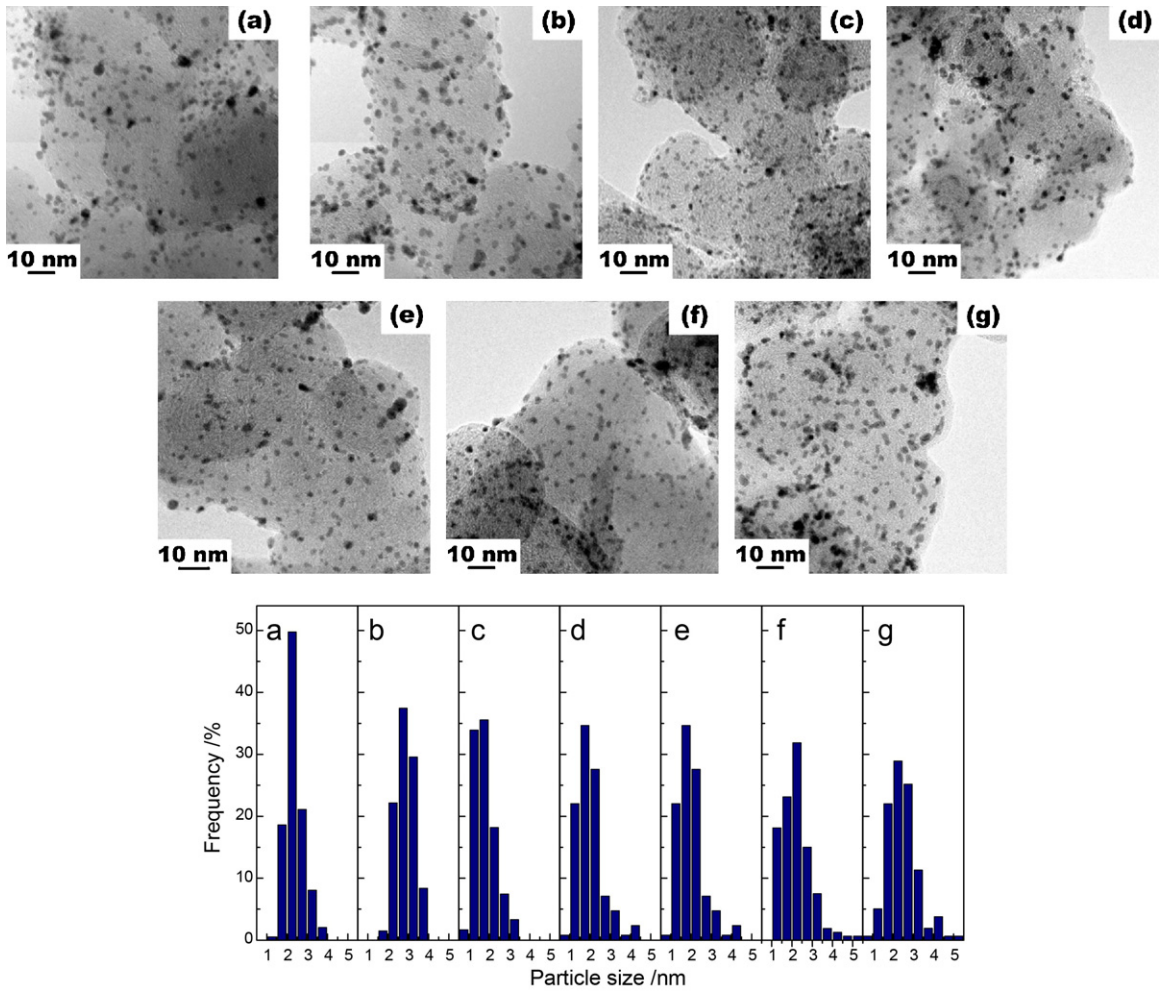

Fig. 1. TEM images and particle size distributions for Pt-CA-$NaBH_4$ (a), Pt_3Fe-CA-$NaBH_4$ (b), Pt-MI (c), Pt_4Fe-MI (d), Pt_3Fe-MI (e), Pt_2Fe-MI (f), and PtFe-MI (g) catalysts.

and 2.9 nm, respectively. The two catalysts still had slightly bigger particle sizes than the corresponding Pt-MI and Pt_3Fe-MI.

The XRD patterns of the carbon-supported Pt and Pt–Fe catalysts are shown in Fig. 2. The characteristic diffraction peaks of the face-centered cubic (fcc) crystal structure are clearly seen in the XRD patterns of Pt-CA-$NaBH_4$ and Pt_3Fe-CA-$NaBH_4$. The Pt and Pt–Fe catalysts prepared by the MI method had distinctly broader diffraction peaks, and the two peaks of the (1 1 1) and (2 0 0) crystalline planes almost merged into one single peak. Thus, according to the Scherrer formula, these catalysts had smaller mean particle sizes than those of Pt-CA-$NaBH_4$ and Pt_3Fe-CA-$NaBH_4$. This result is consistent with the TEM analysis.

The (2 2 0) diffraction peaks, which are not influenced by the carbon support, were used to determine whether Pt–Fe alloy particles were formed in these Pt–Fe catalysts. The (2 2 0) diffraction peak of the two Pt catalysts and the Pt–Fe catalysts prepared by the MI method were all at about 67.5°. The Bragg formula was used to calculate the lattice parameters. The lattice parameters of these catalysts were approximately 0.3926 nm. This indicates that there were almost no Pt–Fe alloy particles in the Pt–Fe catalysts prepared by the MI method. However, the (2 2 0) diffraction peaks were distinctly shifted to a higher angle, 68.4°, for Pt_3Fe-CA-$NaBH_4$ and the lattice parameter was 0.3875 nm. It can be seen that a Pt–Fe alloy was formed in Pt_3Fe-CA-$NaBH_4$.

The Pt and Fe precursors had different redox potentials in EG and could not be reduced to metallic Pt and Fe at the same time in the MI method. Pt–Fe alloy particles were therefore not easily formed. Sodium citrate can coordinate strongly via its carboxyl groups. When sodium citrate was introduced, Pt and Fe chelate-type complexes were formed [20,23]. The redox potentials of the Pt and Fe precursors were also changed and became close to each other. The two precursors could be synchronously reduced. Thus, the Fe atoms partly entered into the Pt lattice [25–27] and a Pt–Fe alloy was found in Pt_3Fe-CA-$NaBH_4$.

XPS was used to analyze the surface chemical states of the metal particles in the Pt/C and Pt_3Fe/C catalysts. Fig. 3 presents the XPS spectra for the Pt 4f region. The Pt 4f signal can be deconvoluted to three pairs of doublets (Pt $4f_{7/2}$ and Pt $4f_{5/2}$) in all of the catalysts [28]. The first doublet pair at 71.4–71.5 eV (Pt $4f_{7/2}$) and 74.7–74.8 eV (Pt $4f_{5/2}$) is assigned to metallic Pt. The doublet with binding energies of 72.4 eV and 75.5–75.8 eV is attributed to PtO or $Pt(OH)_2$. The additional peaks (73.7–73.8 eV and 77.3–77.4 eV) arise from higher oxidation species, PtO_2.

Fig. 4 shows the XPS spectra for the Fe 2p region. The peaks of Fe $2p_{3/2}$ (about 711 eV) and Fe $2p_{1/2}$ (about 721 eV) can be observed. The intensities of the two peaks were very weak, and the Fe $2p_{1/2}$ peak suffered serious interference by the Pt 4s peak (about 726 eV). The relative contents of the Fe components with different valence states cannot be accurately analyzed. However, it can be qualitatively determined that the Fe $2p_{3/2}$ peak for Pt_3Fe-CA-$NaBH_4$ had a slightly lower binding energy than that for Pt_3Fe-MI. Thus, there were more Fe oxides species in the Pt_3Fe-MI catalyst.

The binding energies of the Pt components and their relative intensities are listed in Table 1. During the preparation of the

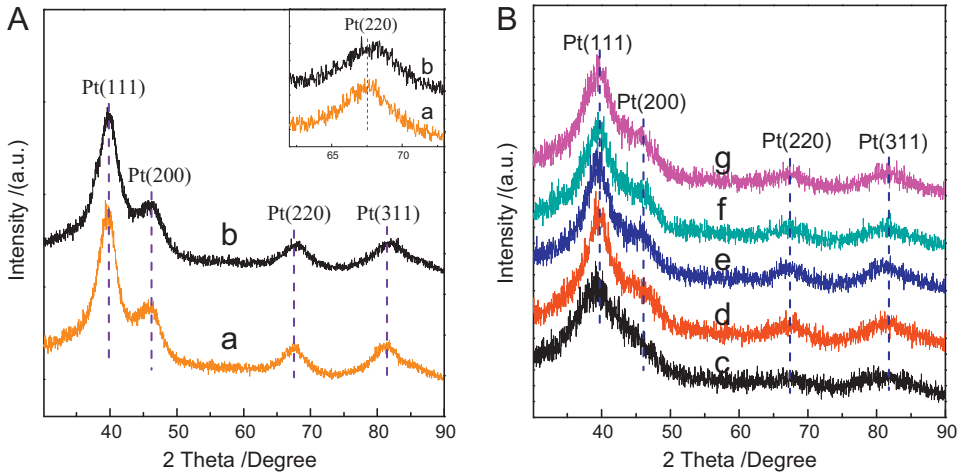

Fig. 2. (A) XRD patterns for the Pt/C (a) and Pt_3Fe/C (b) catalysts prepared by the CA-$NaBH_4$ method. The inset shows the (2 2 0) diffraction peaks of the two catalysts. (B) XRD patterns for the Pt/C (c), Pt_4Fe/C (d), Pt_3Fe/C (e), Pt_2Fe/C (f) and PtFe/C (g) catalysts prepared by the MI method.

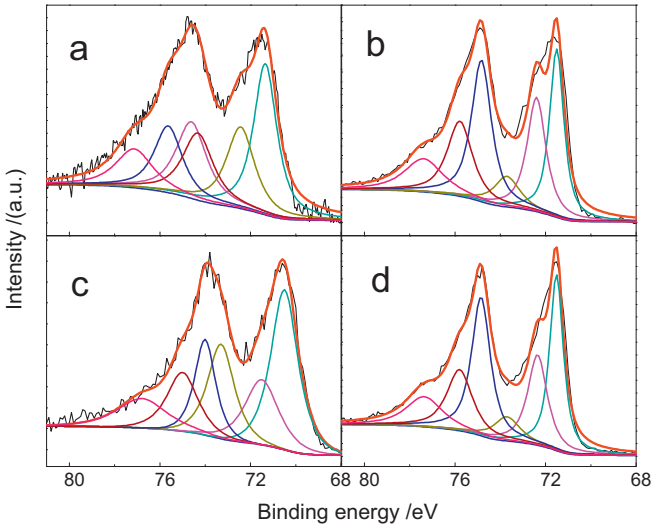

Fig. 3. Deconvoluted Pt 4f XPS core level spectra of the Pt/C (a and b) and Pt_3Fe/C (c and d) catalysts prepared by different methods: MI (a and c) and CA-$NaBH_4$ (b and d).

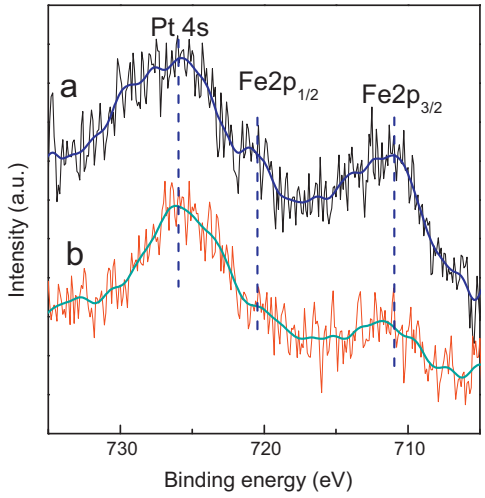

Fig. 4. Fe 2p XPS core level spectra of the Pt_3Fe/C catalysts prepared by different methods: CA-$NaBH_4$ (a) and MI (b).

carbon-supported Pt–Fe catalysts, most Pt and Fe precursor ions were reduced to metallic species in the synthesis solution. The obtained Pt and Pt–Fe catalysts were exposed to air during subsequent operations such as drying at 105 °C. The metallic Pt and Fe existing in the nanoparticles would be partially oxidized in these steps. The metallic Fe was more easily oxidized than the metallic Pt. The oxidation of the metallic Fe would hold back the oxidation of the metallic Pt to some extent. Thus, The Pt–Fe catalyst had more metallic Pt species than did the Pt catalyst prepared by the same procedure. In Pt_3Fe-MI, there were no alloyed Pt–Fe particles and the Fe particles existed independently. It can be deduced that most Fe particles in the size range 0.5–5.5 nm would be oxidized, and that the Fe would exist mainly as oxides.

3.2. Performances of hydrophobic catalysts

The Pt/C and Pt–Fe/C catalysts prepared by the MI and CA-$NaBH_4$ methods were loaded onto an FN carrier to fabricate hydrophobic catalysts. The catalytic activities of the obtained hydrophobic catalysts were tested for LPCE. As shown in Fig. 5, the catalytic activity of Pt-MI-H was higher than that of Pt-CA-$NaBH_4$-H. During the preparation of Pt-CA-$NaBH_4$, the CA, a strong capping agent, can adsorb on the surface of the Pt nanoparticles and cover some active sites. Consequently, the activity of the Pt-CA-$NaBH_4$-H would be reduced [20]. However, our previous research proved that the CA has little influence on the activities of the resulting hydrophobic catalysts because of the post-treatment at high temperature [29]. The Pt-MI-H catalysts had smaller Pt particle sizes and larger

Table 1
Binding energies and relative intensities of various species as obtained from the Pt 4f XPS spectra of the Pt/C and Pt_3Fe/C catalysts prepared by different methods.

Catalyst sample	Pt species	Binding energy (eV)	Relative intensity (%)
Pt-CA-$NaBH_4$	Pt^0	71.5, 74.8	46.3
	Pt^{2+}	72.4, 75.8	35.5
	Pt^{4+}	73.7, 77.4	18.1
Pt_3Fe-CA-$NaBH_4$	Pt^0	71.5, 74.8	49.9
	Pt^{2+}	72.4, 75.8	32.9
	Pt^{4+}	73.7, 77.4	17.2
Pt-MI	Pt^0	71.4, 74.7	40.9
	Pt^{2+}	72.4, 75.6	32.9
	Pt^{4+}	73.8, 77.4	26.1
Pt_3Fe-MI	Pt^0	71.3, 74.7	42.7
	Pt^{2+}	72.4, 75.5	31.2
	Pt^{4+}	73.7, 77.3	26.5

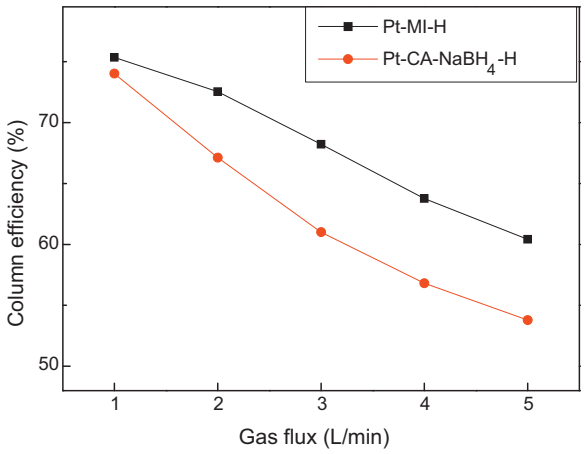

Fig. 5. Catalytic activities of hydrophobic Pt catalysts prepared by MI and CA-$NaBH_4$ methods.

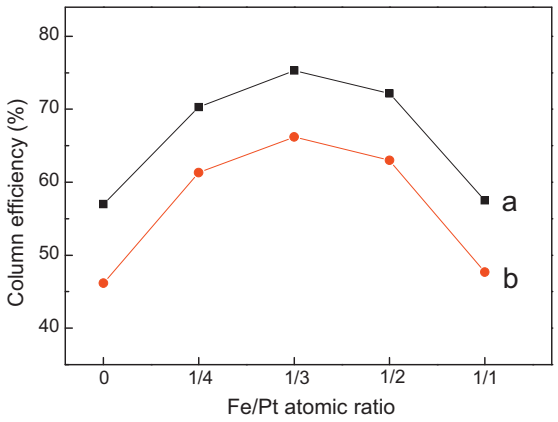

Fig. 7. Catalytic activities of Pt-based and Pt–Fe-based hydrophobic catalysts with different Fe/Pt molar ratios at different hydrogen gas fluxes: 2 L min^{-1} (a) and 4 L min^{-1} (b).

reaction interfaces than did Pt-CA-$NaBH_4$-H. This is the main reason why Pt-MI-H showed higher LPCE catalytic activity [7].

The activities of the two hydrophobic Pt_3Fe catalysts were analyzed and compared with those of the pure Pt hydrophobic catalysts. As shown in Fig. 6, the activity of Pt_3Fe-MI-H was enhanced as a result of the addition of a second element, Fe. However, the catalytic activity of Pt_3Fe-CA-$NaBH_4$-H was slightly lower than that of Pt-CA-$NaBH_4$-H.

Based on the MI methods, hydrophobic Pt–Fe catalysts with different Fe/Pt molar ratios were fabricated. Each hydrophobic catalyst had an equal weight percentage of Pt. Fig. 7 presents the LPCE catalytic activities of these hydrophobic catalysts. It can be seen that all the hydrophobic catalysts, with Fe/Pt molar ratios ranging from 1/4 to 1/1, had higher catalytic activities than that of Pt-MI-H. The Pt_3Fe-MI-H catalyst showed the highest column efficiency under the same experimental conditions. The activities of the hydrophobic catalysts decreased with further decreases or increases in the Fe/Pt molar ratio.

The pure Pt hydrophobic catalysts contain metallic Pt and Pt oxides. According to previous reports [5,6], there are two reaction pathways on the different Pt species for LPCE. On the surface of metallic Pt, water molecules cannot be dissociated to —OA and —A (A represents a hydrogen isotope atom) [30–32]. The hydrogen isotope exchange reaction occurs via hydrated intermediates such as $A_5O_2^+$, $A_7O_3^+$, and $A_9O_4^+$ (Route 1) [33]. There is also another reaction pathway on the Pt oxides. As a result of dissociation of the water molecules, the reaction happens through direct exchange of the formed hydrogen isotope atoms (Route 2). Reaction Route 1 is the primary reaction pathway for LPCE. However, the two reaction routes can be promoted by one another.

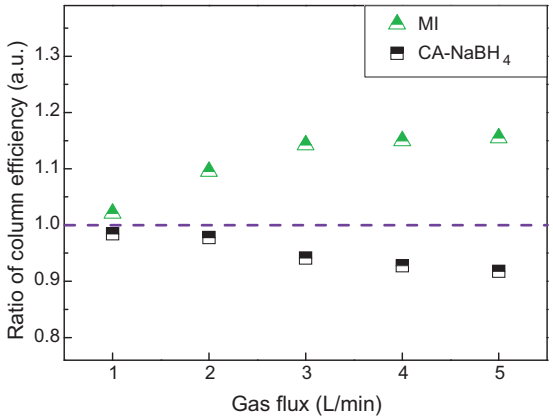

Fig. 6. Ratios of the column efficiencies of Pt_3Fe-MI-H to Pt-MI-H, and Pt_3Fe-CA-$NaBH_4$-H to Pt-CA-$NaBH_4$-H for LPCE. The four hydrophobic catalysts had equal Pt contents.

As discussed above, a Pt–Fe alloy is formed in the Pt_3Fe-MI-H catalyst. As a consequence, the electronic structure of the Pt would be changed. The LPCE reaction rate was also influenced by the primary reaction pathway, namely Route 1. This may be why the catalytic activity of Pt_3Fe-MI-H was lower than that of Pt-MI-H. Further research is necessary to elucidate the details of the reaction mechanism.

For Pt_3Fe-MI-H, there were no alloyed Pt–Fe particles and the Fe existed mostly as oxides. Water molecules are easily dissociated on the surface of Fe oxide species. The addition of Fe oxide species will facilitate Route 2, and hence the reaction rate via Route 2 will be accelerated [6]. Simultaneously, a spillover transfer effect of —OA from M—OA (M is a Fe oxide species) to metallic Pt will take place [34–36]. Thus, Route 1 is promoted by Route 2, which results in enhanced activity of the Pt_3Fe-MI-H catalyst. It has also been reported that the introduction of hydrous Ru oxide can improve the LPCE catalytic performance of pure Pt [6]. Fe oxides and hydrous Ru oxides have similar effects.

4. Conclusions

Carbon-supported Pt and Pt–Fe catalysts were prepared by the MI and CA-$NaBH_4$ methods. Highly dispersed Pt/C and Pt–Fe/C catalysts were obtained. Pt-CA-$NaBH_4$ and Pt_3Fe-CA-$NaBH_4$ had slightly larger mean particle sizes. A Pt–Fe alloy was formed in Pt_3Fe-CA-$NaBH_4$ as a result of the introduction of the strong chelating agent CA in the reaction solution. More Fe oxides species therefore existed in Pt_3Fe-MI than in Pt_3Fe-CA-$NaBH_4$.

The corresponding hydrophobic catalysts were then fabricated and the catalytic activities were tested for LPCE. The activities of the Pt-Fe-MI-H catalysts with different Fe/Pt molar ratios increased as a result of the addition of Fe; Pt_3Fe-MI-H had the highest catalytic activity. This was explained by the reaction mechanisms of the double route for LPCE catalysis. However, the catalytic activity of Pt_3Fe-CA-$NaBH_4$-H was slightly lower than that of Pt-CA-$NaBH_4$-H. The formation of a Pt–Fe alloy was a possible reason.

Acknowledgments

We are grateful for financial support from the National Magnetic Confinement Fusion Science Program (No. 2011GB11102) and the National Natural Science Foundation of China (No. 20901071).

References

[1] A.N. Perevezentsev, A.C. Bell, Detritiation studies for JET decommissioning, Fusion Sci. Technol. 53 (2008) 816–829.
[2] I. Cristescu, I.R. Cristescu, L. Dörr, M. Glugla, G. Hellriegel, R. Michling, D. Murdoch, P. Schäfer, S. Welte, W. Wurster, Commissioning of water detritiation and cryogenic distillation systems at TLK in view of ITER design, Fusion Eng. Des. 82 (2007) 2126–2132.
[3] K.R. Kim, M.S. Lee, S. Paek, S.P. Yim, D.H. Ahn, H. Chung, Operational analysis of a liquid phase catalytic exchange column for a detritiation of heavy water, Sep. Purif. Technol. 54 (2007) 410–414.
[4] K.M. Song, S.H. Sohn, D.W. Kang, S.W. Paek, D.H. Ahn, Installation of liquid phase catalytic exchange columns for the Wolsong tritium removal facility, Fusion Eng. Des. 82 (2007) 2264–2268.
[5] S. Hu, L.P. Xiong, X.B. Ren, C.B. Wang, Y.M. Luo, Pt–Ir binary hydrophobic catalysts: effects of Ir content and particle size on catalytic performance for liquid phase catalytic exchange, Int. J. Hydrogen Energy 34 (2009) 8723–8732.
[6] S. Hu, L.P. Xiong, J.W. Hou, K.P. Weng, Y.M. Luo, T.Z. Yang, The roles of metals and their oxide species in hydrophobic Pt–Ru catalysts for the interphase H/D isotope separation, Int. J. Hydrogen Energy 35 (2011) 10118–10126.
[7] S. Hu, C.J. Xiao, Z.L. Zhu, S.Z. Luo, H.Y. Wang, Y.M. Luo, X.B. Ren, Highly dispersed hydrophobic Pt/C/FN catalysts: preparations and effect of Pt particle size on hydrogen–water liquid phase exchange reaction, Acta Chim. Sin. 65 (2007) 2515–2521.
[8] I. Popescu, Gh. Ionita, I. Stefanescu, C. Varlam, D. Dobrinescu, I. Faurescu, Improved characteristics of hydrophobic polytetrafluoroethylene–platinum catalysts for tritium recovery from tritiated water, Fusion Eng. Des. 83 (2008) 10–12.
[9] S. Paek, D.H. Ahn, H.J. Choi, K.R. Kim, M. Lee, S.P. Yim, H. Chung, K.M. Song, S.H. Sohn, The performance of a trickle-bed reactor packed with a Pt/SDBC catalyst mixture for the CECE process, Fusion Eng. Des. 82 (2007) 2252–2258.
[10] J. Li, S. Suppiah, K. Kutchcoskie, Wetproofed catalysts for hydrogen isotope exchange, US Patent No. 2005/0181938 A1 (2005).
[11] W.H. Stevens, Process and catalyst for enriching a fluid with hydrogen isotopes, CA Patent No. 907 292 (1972).
[12] W. Chen, J. Kim, S. Sun, S. Chen, Composition effects of FePt alloy nanoparticles on the electro-oxidation of formic acid, Langmuir 23 (2007) 11303–11310.
[13] J. Xu, K. Hua, G. Sun, C. Wang, X. Lv, Y. Wang, Electrooxidation of methanol on carbon nanotubes supported Pt–Fe alloy electrode, Electrochem. Commun. 8 (2006) 982–986.
[14] C.T. Hsieh, J.Y. Lin, Fabrication of bimetallic Pt–M (M = Fe, Co, and Ni) nanoparticle/carbon nanotube electrocatalysts for direct methanol fuel cells, J. Power Sources 188 (2009) 347–352.
[15] J.W. Kim, B. Lim, H.S. Jang, S.J. Hwang, S.J. Yoo, J.S. Ha, E.A. Cho, T.H. Lim, S.W. Nam, S.K. Kim, Size-controlled synthesis of Pt nanoparticles and their electrochemical activities toward oxygen reduction, Int. J. Hydrogen Energy 36 (2011) 706–712.
[16] C.T. Hsieh, W.M. Hung, W.Y. Chen, J.Y. Lin, Microwave-assisted polyol synthesis of Pt–Zn electrocatalysts on carbon nanotube electrodes for methanol oxidation, Int. J. Hydrogen Energy 36 (2011) 2765–2772.
[17] X. Li, W.X. Chen, J. Zhao, W. Xing, Z.D. Xu, Microwave polyol synthesis of Pt/CNTs catalysts: effects of pH on particle size and electrocatalytic activity for methanol electrooxidization, Carbon 43 (2005) 2168–2174.
[18] C. Bock, C. Paquet, M. Couillard, G.A. Botton, B.R. Macougall, Size-selected synthesis of PtRu nano-catalysts: reaction and size control mechanism, J. Am. Chem. Soc. 126 (2004) 8028–8037.
[19] L.S. Sarma, C.H. Chen, S.M.S. Kumar, G.R. Wang, S.C. Yen, D.G. Liu, H.S. Sheu, K.L. Yu, T.S. Tang, J.F. Lee, C. Bock, K.H. Chen, B.J. Hwang, Formation of Pt–Ru nanoparticles in ethylene glycol solution: an in situ X-ray absorption spectroscopy study, Langmuir 23 (2007) 5802–5809.
[20] J. Zeng, J.Y. Lee, W. Zhou, Activities of Pt/C catalysts prepared by low temperature chemical reduction methods, Appl. Catal. A: Gen. 308 (2006) 99–104.
[21] J. Lobato, P. Cañizares, M.A. Rodrigo, J.J. Linares, Study of different bimetallic anodic catalysts supported on carbon for a high temperature polybenzimidazole-based direct ethanol fuel cell, Appl. Catal. B: Environ. 91 (2009) 269–274.
[22] Y. Tang, H. Zhang, H. Zhong, T. Xu, H. Jin, Carbon-supported Pd–Pt cathode electrocatalysts for proton exchange membrane fuel cells, J. Power Sources 196 (2011) 3523–3529.
[23] Z. Bai, L. Yang, J. Zhang, L. Li, C. Hu, J. Lv, Y. Guo, High-efficiency carbon-supported platinum catalysts stabilized with sodium citrate for methanol oxidation, J. Power Sources 195 (2010) 2653–2658.
[24] J. Ge, W. Xing, X. Xue, C. Liu, T. Lu, J. Liao, Controllable synthesis of Pd nanocatalysts for direct formic acid fuel cell (DFAFC) application: from Pd hollow nanospheres to Pd nanoparticles, J. Phys. Chem. C 111 (2007) 17305–17310.
[25] Y. Tang, S. Cao, Y. Chen, T. Lu, Y. Zhou, T. Lu, J. Bao, Effect of Fe state on electrocatalytic activity of Pd–Fe/C catalyst for oxygen reduction, Appl. Surf. Sci. 256 (2010) 4196–4200.
[26] Y. Chen, Y. Zhou, Y. Tang, T. Lu, Electrocatalytic properties of carbon-supported Pt–Ru catalysts with the high alloying degree for formic acid electrooxidation, J. Power Sources 195 (2010) 4129–4134.
[27] Y. Chen, Y. Tang, C. Liu, W. Xing, T. Lu, Room temperature preparation of carbon supported Pt–Ru catalysts, J. Power Sources 161 (2006) 470–473.
[28] J.L. Gómez de la Fuente, M.V. Martínez-Huerta, S. Rojas, P. Hernández-Fernández, P. Terreros, J.L.G. Fierro, M.A. Peña, Tailoring and structure of PtRu nanoparticles supported on functionalized carbon for DMFC applications: new evidence of the hydrous ruthenium oxide phase, Appl. Catal. B: Environ. 88 (2009) 505–514.
[29] J.W. Hou, L.P. Xiong, K.P. Weng, S. Hu, Y.M. Luo, Pt/C catalysts: microwave-irradiated polyol method synthesis and catalytic activities for hydrogen–water liquid exchange reaction, Atom. Energy Sci. Technol. 46, in press.
[30] S. Meng, L.F. Xu, E.G. Wang, S. Gao, Vibrational recognition of hydrogen-bonded water networks on a metal surface, Phys. Rev. Lett. 89 (2002), 176104. 1–4.
[31] M.L. Grecea, E.H.G. Backus, B. Riedmuller, A. Eichler, A.W. Kleyn, M. Bonn, The interaction of water with the Pt(5 3 3) surface, J. Phys. Chem. B 108 (2004) 12575–12582.
[32] H. Ogasawara, B. Brena, D. Nordlund, M. Nyberg, A. Pelmenschikov, L.G.M. Pettersson, A. Nilsson, Structure and bonding of water on Pt(1 1 1), Phys. Rev. Lett. 89 (2002), 276102. 1–4.
[33] R.I. Masel, P. Blowers, N. Chen, Formation of hydronium and water–hydronium complexes during coadsorption of hydrogen and water on (2 × 1) Pt(1 1 0), Surf. Sci. 419 (1999) 150–157.
[34] J.M. Jaksic, D. Labou, C.M. Lacnjevac, A. Siokou, M.M. Jaksic, Potentiodynamic estimation of key parametric criterions and interrelating reversible spillover effects for electrochemical promotion, Appl. Catal. A: Gen. 380 (2010) 1–14.
[35] J.M. Jaksic, N.V. Krstajic, L.M. Vracar, S.G. Neophytides, D. Labou, P. Falaras, M.M. Jaksic, Spillover of primary oxides as a dynamic catalysts effect of interactive hypo-d-oxide supports, Electrochim. Acta 53 (2007) 349–361.
[36] N.V. Krstajic, L.M. Vracar, V.R. Radmilovic, S.G. Neophytides, D. Labou, J.M. Jaksic, R. Tunold, P. Falaras, M.M. Jaksic, Advances in interactive supported electrocatalysts for hydrogen and oxygen electrode reactions, Surf. Sci. 601 (2007) 1949–1966.